RESEARCH

Highly dispersed cobalt Fischer–Tropsch synthesis catalysts supported on γ-Al$_2$O$_3$, CNTs, and graphene nanosheet using chemical vapor deposition

Iraj Kazemnejad[1] · Alireza Feizbakhsh[1] [ORCID] · Ali Niazi[1] · Ahmad Tavasoli[2]

Abstract

Highly dispersed 15.0 wt% cobalt catalysts were prepared on γ-Al$_2$O$_3$, carbon nanotubes (CNTs), and graphene nanosheet (GNS) using chemical vapor deposition (CVD) procedure. The physico-chemical properties of the catalysts were studied by inductively coupled plasma (ICP), Brunauer–Emmett–Teller (BET), X-ray powder diffraction (XRD), field-emission scanning electron microscopy (FESEM), and temperature-programmed reduction (TPR) techniques, and the Fischer–Tropsch synthesis (FTS) performance of the catalysts was assessed at 220 °C, 18 bar, H$_2$/CO = 2 and feed flow rate of 45 ml/min g cat. Based on BET results, Co/GNS catalyst provided highest surface area in comparison to the other catalysts. XRD and FESEM results revealed that CVD method prepared smaller particles on GNS compared to the other supports and resulted in the most dispersed metal particles on GNS according to H$_2$-chemisorption results. The performance of Co/Al$_2$O$_3$ catalyst prepared by CVD method was compared with conventional 15 wt% Co/Al$_2$O$_3$ catalyst prepared by impregnation method. The Co/Al$_2$O$_3$ catalyst prepared with CVD method showed 5.3% higher %CO conversion and 2.1% lower C$_5^+$ selectivity as compared with the Co/Al$_2$O$_3$ catalysts prepared by impregnation method. Among three catalysts prepared by CVD, Co/GNS showed higher %CO conversion of 78.4% and C$_5^+$ selectivity of 70.3%. Co/γ-Al$_2$O$_3$ catalyst showed higher stability.

Keywords Chemical vapor deposition · Cobalt · Dispersion · Activity · Selectivity

Introduction

Fischer–Tropsch synthesis (FTS) is a major process in conversion of gas-to-liquids, coal-to-liquids, and biomass-to-liquids. In the FTS, syngas produced from natural gas, coal, or biomass converts to valuable hydrocarbons by hydrogenation of carbon monoxide [1–3]. In the quest for the development of more active catalysts, a rational strategy is to enhance the cobalt dispersion by decreasing the average particle size [4].

In recent years, gas-phase-based methods have attracted a huge attention in catalysts preparation approaches. Chemical vapor deposition (CVD) is mainly an industrial chemical process, which includes a substrate exposed to a single- or multi-component volatile precursor (in gaseous phase) in an inert atmosphere at controlled temperature and pressure. Metal organic chemical vapor deposition (MOCVD) is a potential alternative for making stable and active catalysts with well-developed structure [5]. This technique offers several advantages: (1) allow direct and efficient deposition of active metals by reaction between surface groups of the support and vapors of a suitable volatile compound; (2) small, uniform, well-dispersed, nanocrystallites active metal particles can be formed [6]. The low cost and facile deposition process to control the thickness and morphology of the films on different substrates make CVD an attractive method for catalyst preparation [7]. Dry methods (working in gas/vapor phase) may represent a significant improvement over wet methods [8]. Among dry methods, chemical vapor deposition (CVD) is known to generate more active and selective catalysts compared to conventional techniques [9].

Alumina is one of the most common supports for FT catalysts and carbon materials such as carbon nanotubes and graphene have also been recently applied for supporting iron

✉ Alireza Feizbakhsh
arafeizbakhsh@gmail.com

[1] Department of Chemistry, Central Tehran Branch, Islamic Azad University, Tehran, Iran

[2] School of Chemistry, College of Science, University of Tehran, Tehran, Iran

and cobalt catalysts [10–12]. To best of our knowledge, gas-phase methods for preparing cobalt catalysts on oxide and carbonous supports and evaluating their performance and stability in FTS have not been studied widely [13]. Cobalt and iron are proposed metal catalysts as the first catalysts for FTS. These catalysts have been employed in industrial processes for hydrocarbon synthesis. Cobalt catalysts are more expensive than iron catalysts, but they are resistant to deactivation. Cobalt-supported catalysts in FTS are usually prepared by impregnation. In this method, cobalt is deposited on porous support in which a dry support is contacted with a solution containing dissolved cobalt precursors. The distribution of cobalt ions on the surface of the support after impregnation is affected by some electrostatic interactions and van der Waals interactions that occur between the nanoparticles and results in the complex particle dynamics manifesting in deposition patterns on the support material [14]. In the previous studies, cobalt precursors have been dispersed on different porous carriers such as SiO_2, Al_2O_3, and TiO_2. The concentration, nature, and distribution of hydroxyl groups play an important role in the genesis of the dispersion of supported metal. Porous supports such as silica, alumina, and titanium have different points of zero charges, and should be pretreatment before use [15]. The concentration of hydroxyl groups can be controlled by pretreatment of the support with some organic compounds such as 1-propanol prior to impregnation resulted in higher metal dispersion and better activity in the FT reaction [16–18]. Carbon materials can be used as catalysts support due to special properties including high surface area, high mechanical strength, chemical inertness, and possibility of using in both basic and acidic solutions. Graphene is a one-atom-thick planar sheet of sp^2-carbon atoms a crystal lattice. The unique specifications of graphene have attracted tremendous interest both in academics and industry. Among numerous procedures, chemical vapor deposition method has been introduced to synthesize the graphene from graphite flakes [16]. CVD has chemical reactions of gaseous reactants on the vicinity of a heated substrate surface. This method can provide a nanostructured and functionally coated materials with a special structure to use in different areas [19]. The advantage of this procedure is because of the uniform distribution of cobalt nanoparticles on catalyst support and possibility of a narrow distribution for cobalt particle size. Use of different types of cobalt materials could be explained by their low melting point and high vapor pressures [20].

The aim of the present study is to employ CVD technique to investigate the properties, performance, and stability of cobalt catalysts on different supports in FTS. The main focus is to investigate CVD-prepared catalysts on different promising supports to have the further insights into the CVD approach which could lead to emerging a new and scalable method for preparing the next generation of Co catalysts.

The formation of small cobalt nanoislands greatly increases the number of surface "defect" sites which have been proposed as the catalytically active sites for Fischer–Tropsch synthesis [21].

Experimental

Catalyst preparation

Functionalization of GNS and CNT

5 g of each support including GNS and CNT (purity > 99.5) were refluxed with 100 ml of 30% HNO3 at 120 °C for 16 h to generate OH groups which act as anchoring sites for metal particles on support surface.

Catalysts prepared by CVD method

Certain amounts of cobalt acetylacetonates ($Co(acac)_2$ Alfa Aesar) and support (GNS, CNTs and Al_2O_3) were loaded into sublimation tube. The tube was sealed and connected to a vacuum system. The sublimation tube was slowly ramped to 100 °C and held at 100 °C temperature for 2 h. Then, the temperature increased to 130 °C and held at this temperature for 2 h. Argon was used as the carrier gas. Decomposing the cobalt acetylacetonate Co (acac)$_2$ compound was conducted in flowing argon for 4 h at 350 °C. The catalysts prepared by CVD method were denied as Co/GNS, Co/CNTs, and Co/Al_2O_3.

Catalyst prepared by impregnation method

The aqueous solution of cobalt nitrate ($Co(NO_3)_2 \cdot 6H_2O$) was impregnated on Al_2O_3 as the support. The catalyst was dried at 120 °C for 3 h and calcination was calcined at 350 °C for 4 h. The catalyst prepared by this method denied as ICo/$Al_2O_3.$

Catalyst characterization

The FTIR technique was performed on a Bruker ISS-88. For each adsorption measurement, 0.5–5% of samples mixed with 95–99.5% potassium bromide (KBr) and a transparent pellet was prepared and the infrared beam passed through pellets.

A confocal Raman microscope system with a laser source of 785 nm was used to measure the Raman shift of the support materials.

Cobalt loadings were measured using a Varian VISTA-MPX inductively coupled plasma atomic emission spectroscopy (ICP-AES) system. The mixture including 0.02 g of the catalyst sample in 5 ml of nitric acid (Merck 65%) and 5 ml

hydrochloric acid (Chem-Lab, 37%) stirred at 40–50 °C for 2 h was filtered and then diluted up to 250 ml.

Field-emission scanning electron microscopy (FESEM JEOL-JSM-6700F instrument) was performed on prepared catalysts to analyze the morphology and homogeneity of Co particles. The samples were prepared by dispersing catalyst powder onto a carbon-coated copper grid.

BET surface area measurements were carried out using an ASAP-2010 system from Micrometrics. In each trial, a weight of approximately 0.25 g of sample was degassed at 200 °C for 4 h under 50 mTorr vacuum, and the BET area, pore volume, and average pore radius were determined.

The phases and crystallite sizes of the catalysts was studied using XRD. A Philips analytical X-ray diffractometer (XPert MPD) with monochromatized Cu/Kα radiation, 2θ angles from 20° to 80° recorded the patterns. The crystal size of the Co_3O_4 was calculated using the Scherrer's equation ($2\theta = 36.8°$).

Micrometrics TPD–TPR 2900 system equipped with a thermal conductivity detector (TCD) was used to conduct H_2-TPR. Traces of water and gases were removed from the catalysts by purging a flow of helium at 140 °C. After cooling to 40 °C, TPR of each sample was performed using 5% H_2 in Ar stream at a flow rate of 40 ml/min at atmospheric pressure and a linearly programmed heating (10 °C/min) up to 850 °C.

Metal dispersion and the average active surface area were evaluated using the TPD technique. First, the TPD of hydrogen was conducted, and then, pulses of 10% oxygen in helium were entered to re-oxidize the samples at 400 °C and the extent of reduction was determined. It is to note that during re-oxidation step, GNS and CNTs have not reacted with oxygen which was clear from the absence of CO_2 peak. It was assumed that Co^0 was oxidized to Co_3O_4. The calculations are summarized below [22]:

$$\%\text{Dispersion} = \frac{\text{number of } Co^0 \text{ atoms on surface}}{\text{number of Co atoms in sample}} \times 100,$$

$$\text{Fraction reduced} = \frac{O_2 \text{ uptake (mol } O_2/\text{grcatalyst)} \times \frac{2}{3} \times \text{cobaltatomic weight (58.9332 g/mol)}}{\text{percentage metal}},$$

$$d \text{ (nm)} = \frac{6000}{\text{density} \times \text{maximum area} \times \text{dispersion}}.$$

Catalyst activity test

Catalysts' performance in FTS was examined in a fixed bed reactor. The reactor temperature was recorded and controlled using an internal K type thermocouple and a PID temperature controller. 0.6 g of catalyst diluted with 2.4 g silicon carbide and used for catalytic tests. The desired flows of hydrogen and carbon monoxide were premixed and entered the reaction zone using Brooks 5850 mass flow controllers. After in situ reduction at 400 °C and $H_2 = 30$ ml/min for 18 h, the reactor temperature decreased and FT tests were conducted at 220 °C, 1.8 MPa, $H_2/CO = 2$ and a flow rate of 45 ml/min. Products were removed and passed through two traps, a hot trap (at 100 °C) and a cold trap (at 0 °C). The uncondensed vapor pressure was reduced to atmospheric. The out let gas flow was measured using a bubble flow meter, analyzed by an online GC and used to measure the CO conversion and gaseous products selectivity. The accumulated liquid (wax, oil and aqueous) products were removed every 24 h and analyzed by GC.

# Results and discussion

CNTs and GNS characterization

The infrared (IR) spectrum used to elucidate the structure and identify functional groups. The spectra of the functionalized CNTs and GNS are shown in Fig. 1. The peaks at 2921 cm^{-1}, 1579 cm^{-1}, and 664 cm^{-1} are related to (C–H) (alkanes), (C–C in–ring) (aromatics), and (–C≡C–H:C–H) (alkynes), respectively. In addition, the peaks at 1384 cm^{-1}, 1729 cm^{-1}, and 3446 cm^{-1} are related to (C–O), (C=O) (carboxylic acids), and (OH) groups (alcohols and phenols).

Raman spectroscopy was conducted to identify the graphitic degree of the samples. There are three peaks in GNS pattern (Fig. 1); G at 1585 cm^{-1}, 2D at 2700 cm^{-1}, and D band at 1350 cm^{-1}. The 2D band is characteristics for GNS in Raman spectrum, and the ratio $I_{(2D)}/I_{(G)}$ provides information about support surface [23]. The G peak is due to the bond stretching of all pairs of sp^2 atoms in both rings and chains. The D peak is due to the breathing modes of sp^2 atoms in rings which means that the D band intensity assigns the abundance of defects in the sheet, while the G band is related to the graphitic hexagonal mode and in highly ordered pyrolytic graphite [24]. Higher D/G ratio for GNS in comparison to CNTs (3 vs 1.1), indicates the higher degree of defect sites on the graphene support which consequences more favorable nucleation sites for the metal nanoparticle on support surface.

**Fig. 1** FTIR and Raman spectrum of the functionalized GNS and CNTs
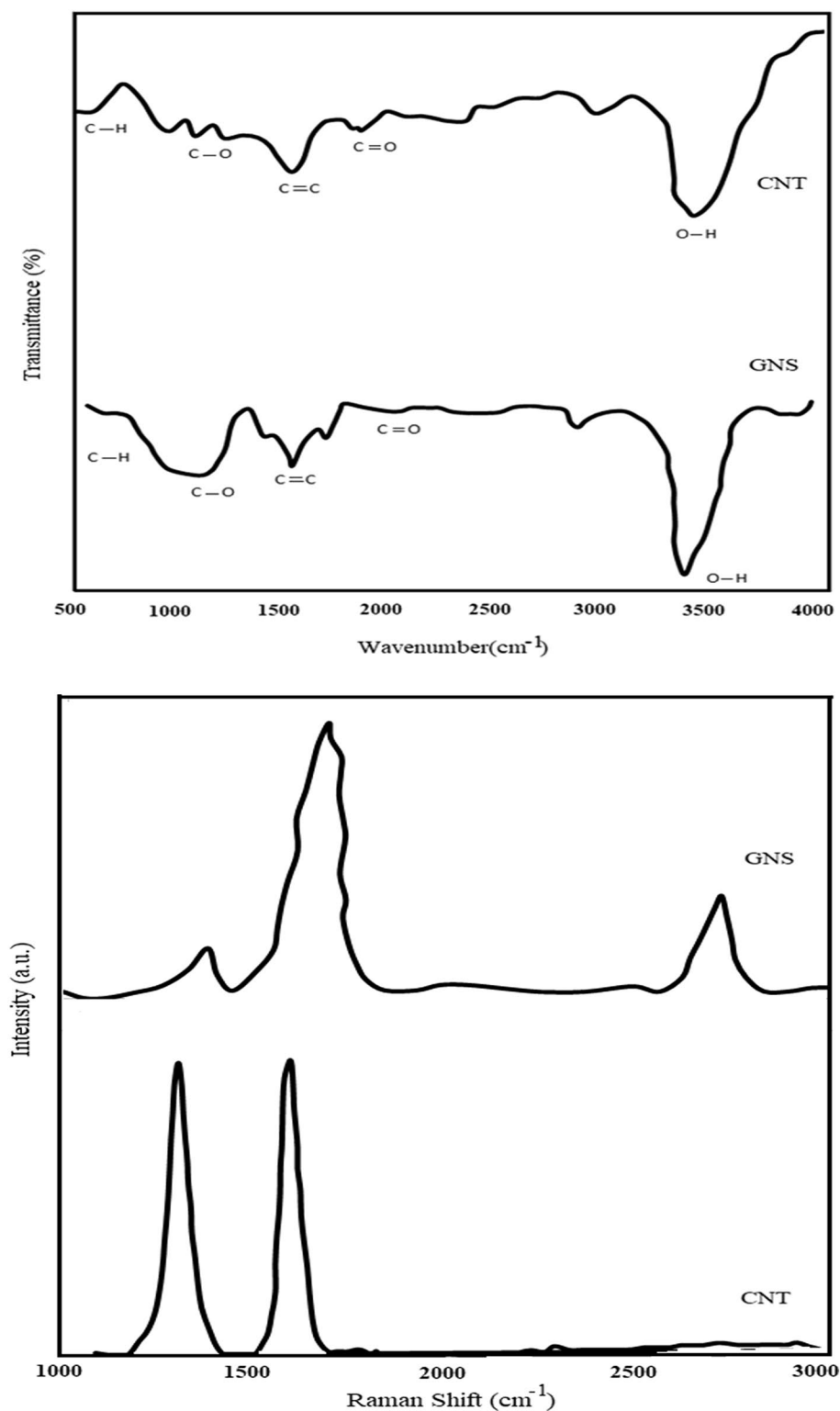
Catalysts' characterization

FESEM images of catalysts are useful for investigating the morphology and also estimating particle-size distributions. The particle-size d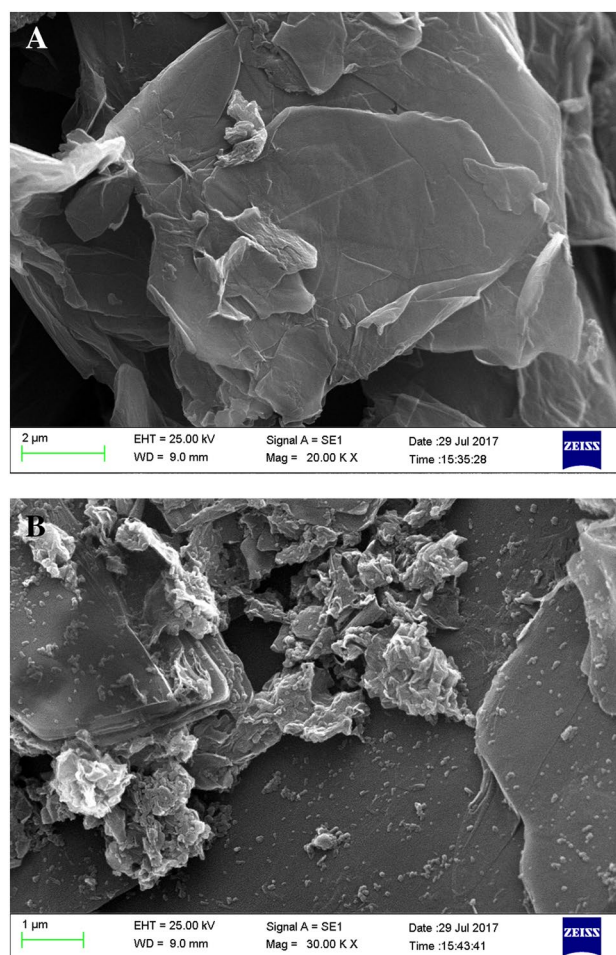istribution was analyzed using ImageJ software and based on FESEM pictures. Figures 2, 3 and 4 present the FESEM pictures of the catalysts prepared by CVD method. The light spots represent the cobalt-oxide species dispersed on supports surface and these species are creating nanoislands. The taken image from the surface of Co/
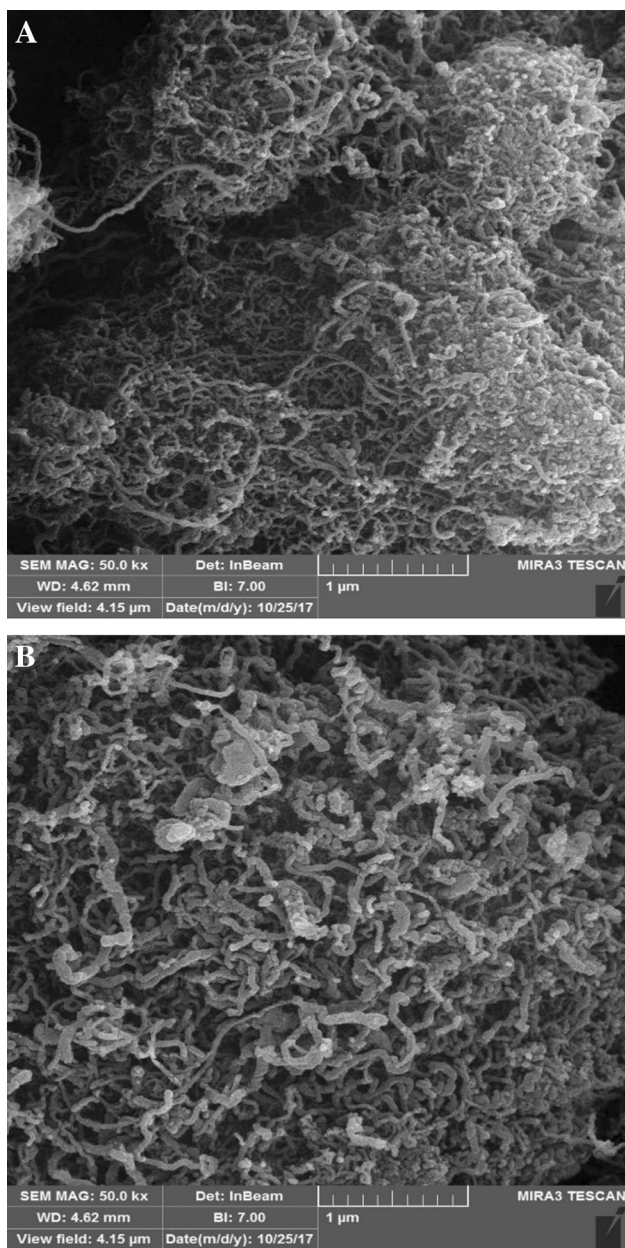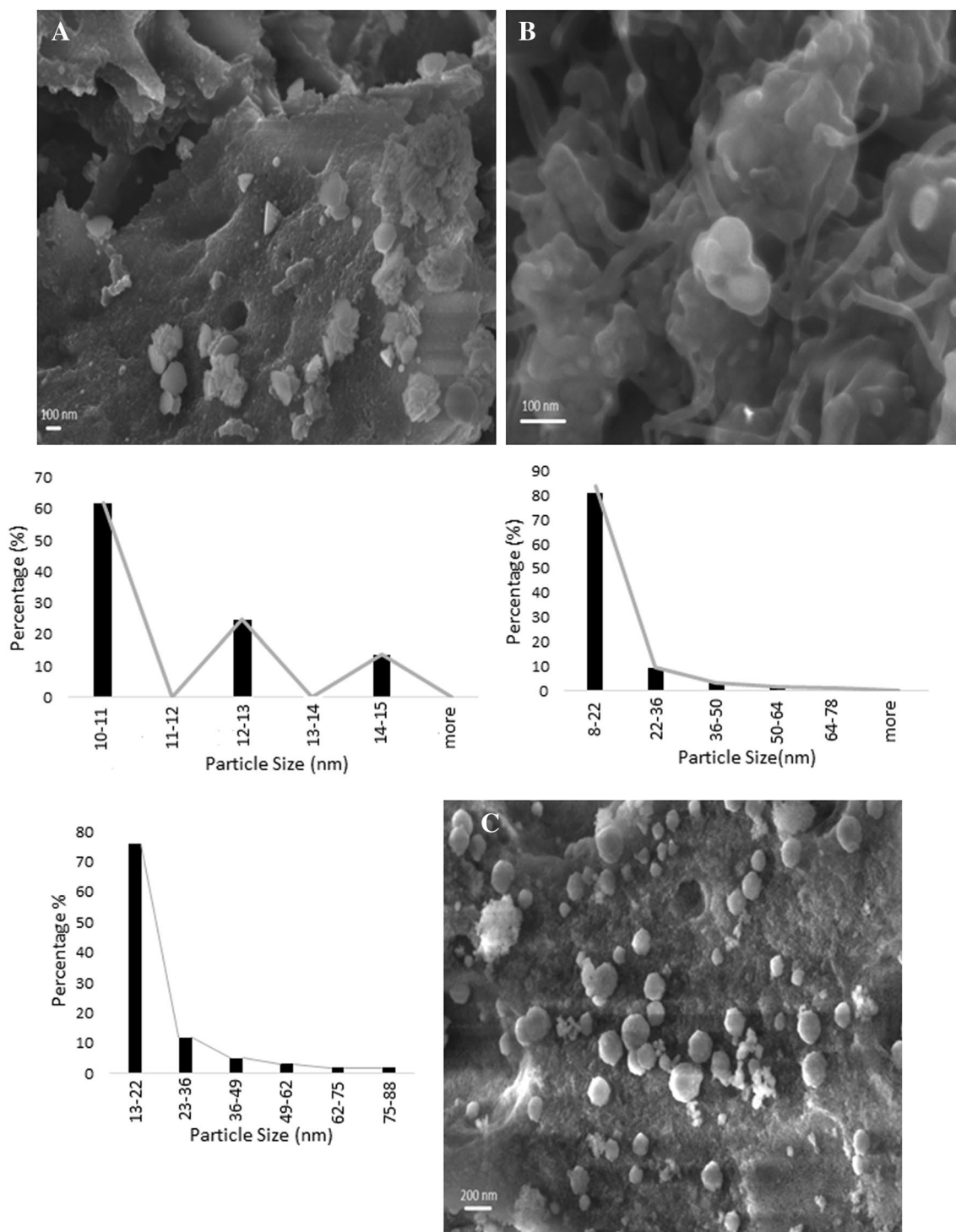
Fig. 2 FESEM images of **a** CNT and **b** Co/CNT

Fig. 3 FESEM images of **a** GNS and **b** Co/GNS

GNS catalyst (Fig. 4a) demonstrates the Co particles which are dispersed on the surface of nanosheets. Particle-size distribution shows small Co particles on graphene sheets. There are particles in the range of 10–15 nm, most between 10 and 11 nm, and the average calculated as 10.7 nm. These results introduce a narrow distribution for Co particles on GNS support. Figure 4b shows the FESEM picture of Co/CNTs catalyst. In this case, cobalt particles are located both at the external surface of small channels and also embedded in inside the tubes. Particle-size distribution diagrams show that particles are distributed with different sizes in a relatively wide range of 8–78 nm and the average is 15.56 nm.

Most parts of the particles are measured between 8 and 22 nm. In Co/Al_2O_3 image (Fig. 5b), the dispersed cobalt was observed on the catalyst granule. In this case, also Co nanoparticles dispersed with a broad size range of 13–88 nm and 76% of metal nanoparticles are located in 13–22 nm domain. Figure 4 also depicts the particle-size diagrams of the cobalt particles, which plotted using the population of cobalt particles on five different FESEM pictures (only one picture is shown here for each catalyst). Different supports resulted in different particle size of cobalt-oxide species in the order of Co/Al_2O_3 > Co/CNTs > Co/GNS, and average Co particles are calculated as 19.3, 15.6, and 10.7 nm, respectively. The image of Co/GNS catalyst shows a lot of edge and corners which are considered as the most active sites in FT reaction. On the other side, the ratio of corner and edges are less in Co/CNTs and Co/Al_2O_3, and this observation could be clearly realized from FESEM images. One of the strategies to create sintering-resistant catalysts is to elongation of the particle-to-particle traveling distance [25]. GNS provide a large surface area compared to CNTs and

Fig. 4 FESEM images of **a** Co/GNS, **b** Co/CNT, and **c** Co/Al$_2$O$_3$ catalysts prepared by CVD method

Al$_2$O$_3$ which could influence the growth of particles. All catalysts are synthesized via similar method and conditions which could affect the establishment of cobalt nanoislands, but support properties to influence the amount, dispersion, and also the properties of these cobalt islands.

Surface area and pore size distribution of the supports and catalysts were studied by BET and results are presented in Table 1. GNS show higher surface area in comparison to CNTs and Al$_2$O$_3$ (400 in comparison to 220 and 200 m^2/g). The BET surface area of the Co/Al$_2$O$_3$, Co/CNTs, and Co/

Fig. 5 XRD patterns of **a** Co/GNS, **b** Co/CNT, and **c** Co/Al$_2$O$_3$ catalysts prepared by CVD method
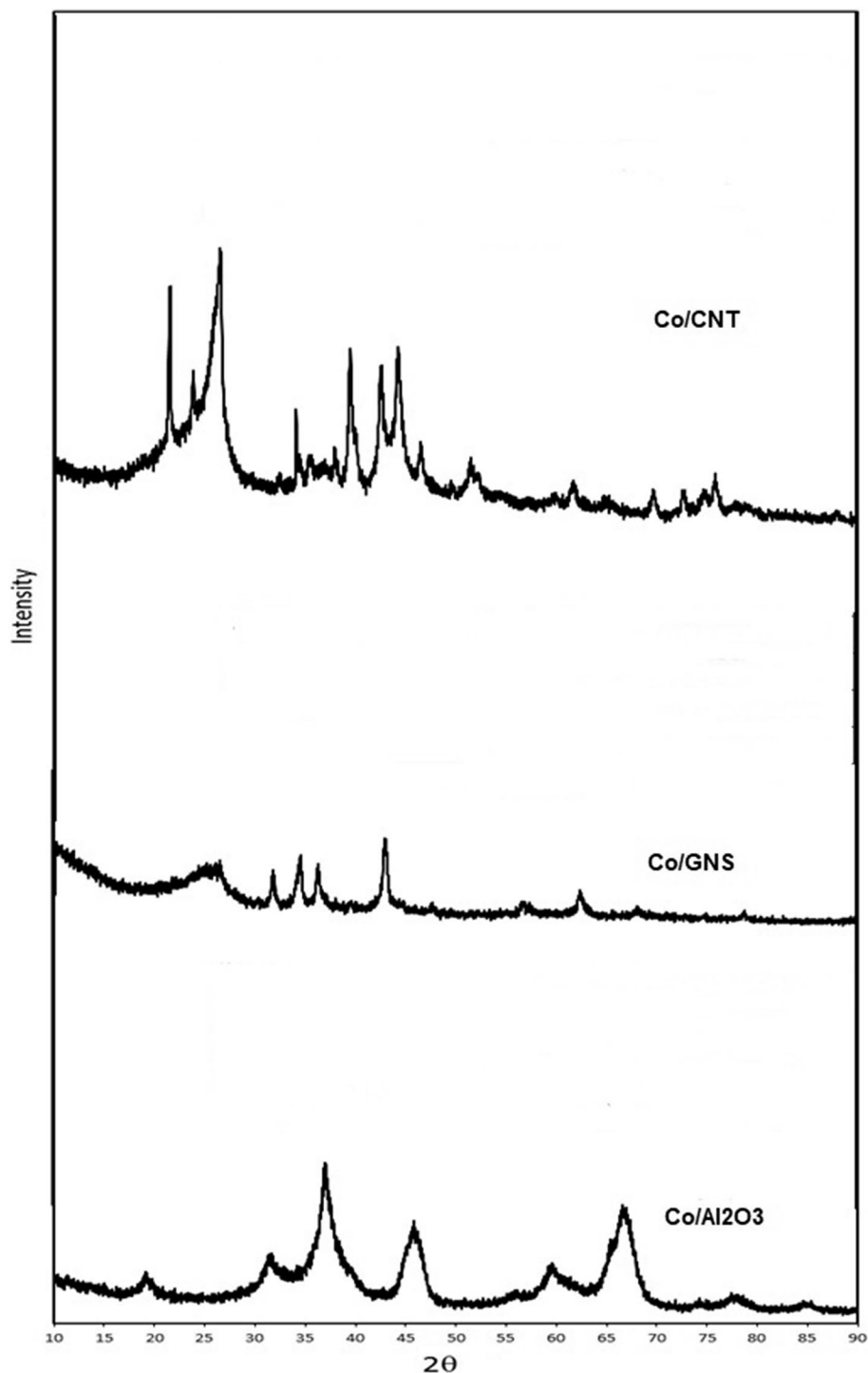
GNS catalysts were 156, 120, and 300 m^2/g, respectively. Blocking of some pores by metal particles causes surface area lose [26]. The cobalt loading of 15.0 wt% equals 20.0 wt% Co$_3$O$_4$ and each support is the only contributor of the surface area. Therefore, theoretical surface area for catalysts could be calculated as follows: ($0.8 \times 412.8 = 330.24$ for Co/GNS), ($0.8 \times 220 = 176$ for Co/CNTs), and ($0.8 \times 200 = 160$ for Co/Al$_2$O$_3$). According to the results,

there are more severe pore blockages in Co/GNS and Co/CNTs in comparison to Co/Al$_2$O$_3$ [27]. Cobalt contents in catalysts were measured and ICP results are also presented in Table 1; the values of deposited Co on GNS, CNTs, and Al$_2$O$_3$ surfaces are 14.0 wt%, 13.9 wt%, and 14.5 wt% which are close to nominal composition of 15.0 wt%.

The XRD patterns of the calcined catalysts are displayed in Fig. 5. In XRD patterns, the sharp peaks are due to the

Table 1 BET surface area and XRD results for the catalysts prepared by CVD method

Catalyst	ICP	BET SA (m^2/g)	Point pore volume (cm^3/g)	Average pore radius (nm)	d_{XRD} (nm)
GNS	–	412.8	0.97	9.5	–
Co/GNS	14.0	300.9	0.860	7.3	10.7
CNTs	–	220	0.88	6.1	–
Co/CNT	13.9	120.5	0.507	6.2	15.56
Al_2O_3	–	200	0.400	6.2	–
Co/Al_2O_3	14.5	156.4	0.385	6.5	19.3

Table 2 Crystallite sizes of cobalt particles determined by H_2 temperatures' programmed desorption and pulse re-oxidation of the catalysts prepared by CVD method

Catalyst	µmol H_2 Desorption g cat.)	µmol O_2 Consumption (g cat.)	%Red.	%Dispersion	d_p (nm) (tot. Co)
Co/CNT	325	236	38.26	29	13.8
Co/GNS	457	298	48.31	39.8	9.8
Co/Al_2O_3	250	198	32.1	22	17.9

crystalline components and the broad features to the amorphous components [28]. Co/GNS and Co/CNTs catalysts present broad peaks at 2θ values of 25° and 43° that suggest the amorphous structure of GNS and CNTs and the rest of the peaks at 31.5°, 36.8°, 44.9°, 59.6° and 65.5° present different crystal planes of the Co_3O_4. These peaks are relatively sharp in all XRD patterns and show the crystalline structure of Co_3O_4 phase. $CoAl_2O_4$ peaks also appeared in XRD pattern of Co/Al_2O_3 catalyst which is related to cobalt-oxide interactions with Al_2O_3 support. The detailed phase analyses are presented in Fig. 5. The Scherrer equation was used to evaluate the size of cobalt-oxide crystallites for the most intense diffraction peak at 2θ of 36.8° (Table 1) [29]. Average crystalline size of cobalt oxides for Al_2O_3, CNTs, and GNS supported catalysts are measured as 10.3, 14.7, and 18.9 nm, respectively. In gaseous reaction, atmosphere, used in CVD method, is a solvent-free area and the particle mobility are limited and also it is to note that the temperature raising is the key point to slow down the particle growth on support surface and decrease particles aggregating during synthesizing. There are considerable metal–support interactions in Co/Al_2O_3 catalyst.

Temperature-programmed reduction (TPR) results are applied for understanding the degree of interaction of the active metals with the supports. Two distinct reduction peaks are related to the reduction of Co_3O_4 to CoO and the CoO to Co^0, respectively [30]. The broad tailing in the TPR spectra resulted from dispersed and probably strongly interacting cobalt species with the supports (specially in Co/Al_2O_3). Using GNS as the support facilitated both reduction steps

in comparison to Co/CNTs and Co/Al_2O_3 catalysts. The first broad reduction step in GNS, CNTs, and Al_2O_3 supported catalysts is centered on 330, 420, and 430 °C, respectively, and second peaks are observed at about 510, 560, and 600 °C. These results could attribute to more defects on graphene surface. Consequently, more functional groups on the graphene surface accelerate the hydrogen spill over in the reduction process [22].

Percentage of dispersion and reduction and also particle diameters are summarized in Table 2. As shown, the hydrogen uptake increases in the order of Co/Al_2O_3 < Co/CNT < Co/GNS. The degree of reduction is obtained as 32.10%, 38.26%, and 48.31% for Co/Al_2O_3, Co/CNTs, and Co/GNS catalysts. These results are in agreement with the TPR outcome and evidence for the improvement of reduction degrees using GNS as support. The dispersion percentage has been calculated as 22%, 29%, and 40% for Co/Al_2O_3, Co/CNT and Co/GNS catalysts. CVD method is a gas-phase preparation method and can provide easy access of the precursor to the interior sites of the support. The amount of anchoring sites on the surface of the support is important and more functional groups on the support generate highly dispersed catalysts [31]. Higher dispersion of smaller cobalt particles will make more cobalt atoms available for FTS reaction.

Fischer–Tropsch synthesis

The results of %CO conversion and selectivity of different products including light and heavy hydrocarbons and CO_2 for ICo/Al_2O_3 and Co/Al_2O_3 catalysts at 220 °C, 1.8 MPa,

Table 3 CO conversion and product selectivities for all the catalysts

Catalyst	CO conversion (%)	CH_4 Selectivity	C2–C4 selectivity (%)	C5+ selectivity (%)	CO_2 selectivity (%)	α
Co/GNS	78.4	20.99	8.31	70.28	0.408	0.77
Co/CNT	60.25	14.45	8.7	72.86	0.9	0.79
Co/Al_2O_3	75.4	11.82	7.6	79.7	0.78	0.83
ICo/Al_2O_3	70.1	10.04	4.2	81.45	0.99	0.86

Reaction conditions: $T = 220$ °C, $P = 1.8$ MPa, H_2/CO = 2, and 0.6 g catalyst

Fig. 6 TPR patterns of **a** Co/GNS, **b** Co/CNTs, and **c** Co/Al$_2$O$_3$ catalysts prepared by CVD method
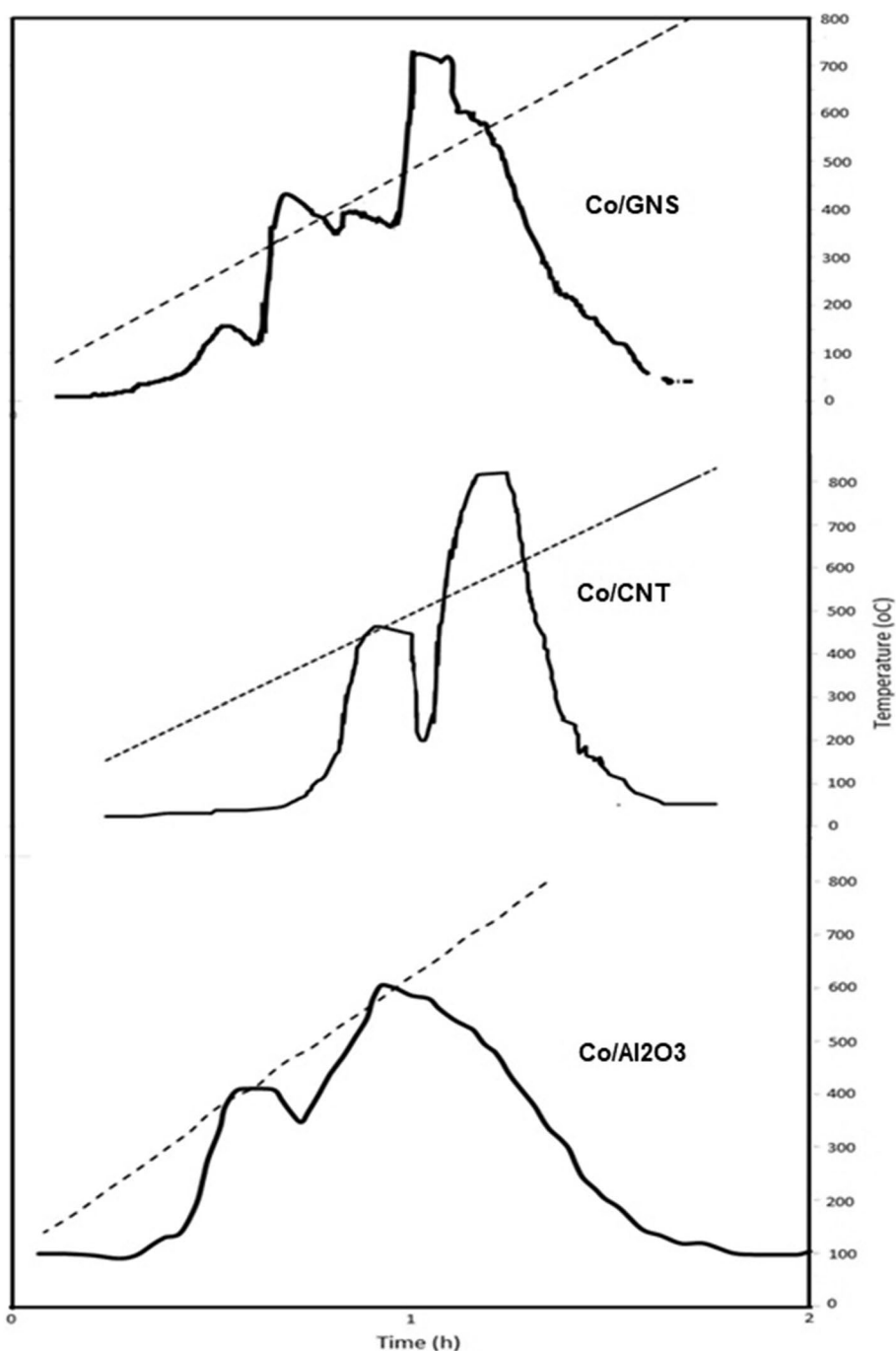

and H$_2$/CO ratio of 2 are presented on Table 3. As shown, using CVD method to prepare the Co/Al$_2$O$_3$ catalyst increased the %CO conversion from 70.1 to 75.4%. Gas-phase preparation methods create well-dispersed metal particles on supports [32]. Higher %CO conversion for Co/Al$_2$O$_3$ catalyst can be attributed to generation of more active sites for the catalyst prepared by CVD method. Increasing C$_5^+$ selectivity is considered as one of the most important aims in designing new catalysts for FTS. Co/Al$_2$O$_3$ catalyst

prepared by CVD method slightly shifted the liquid products selectivity to lighter hydrocarbons.

Table 3 also shows the results of %CO conversion and selectivity of different products in FT reaction at 220 °C, 1.8 MPa, and H$_2$/CO ratio of 2 for the catalysts with different supports prepared by CVD method. CO conversions are calculated as 60.2%, 75.4%, and 78.4% for Co/CNTs, Co/Al$_2$O$_3$, and Co/GNS catalysts (Table 3). CNT supported catalyst showed the lowest percentage CO conversion in

Fig. 7 ASF distribution of FTS products on Co/GNS, Co/CNTs, Co/Al$_2$O$_3$, and ICo/Al$_2$O$_3$ catalysts ($T = 220$ °C, $P = 1.8$ MPa and H$_2$/CO$=2$)
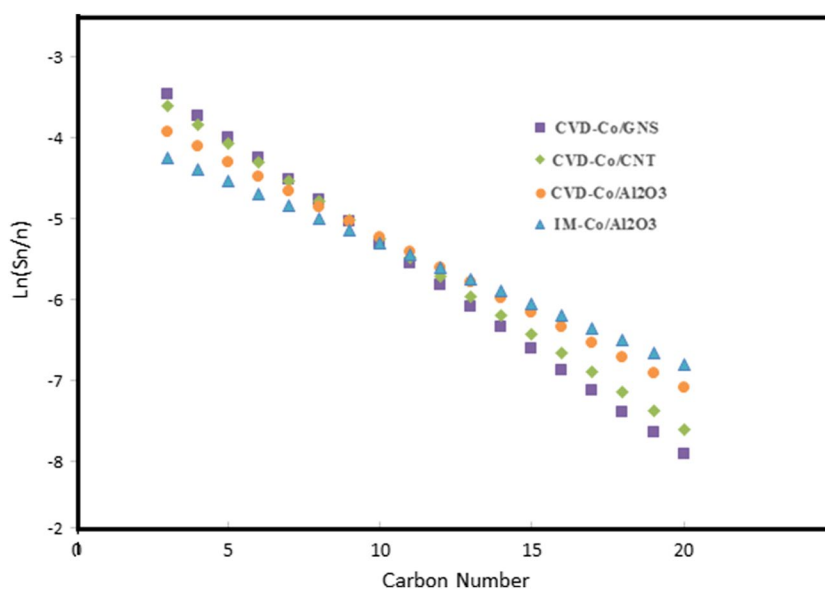
comparison to the other two catalysts prepared using CVD method. In liquid phase-based preparation methods, the capillary forces are effective in introducing metal particles into nanotubes [33]. In gas phase, this force is limited which might weaken the particles permeability into carbon nanotubes. Metal particles inside these tubes are recognized as the most active sites [34]. We assume that lower activity of this catalyst can be related to decreasing the amount of active cobalt particles, because a considerable portion of nanoparticle is located on the outer surface, as the FESEM images show.

Based on the BET and FESEM results, GNS presents nanosheets with a high surface area which consequent smaller distributed cobalt nanoparticles in comparison to other supports. High CO conversion could be related to higher amounts of active sites with high ratio of steps and edges [35]. It is also noteworthy that the steps not only favor CO dissociation but also are advantageous to C/O hydrogenation [36]. TPR and XRD results show relatively high metal–support interactions in Al$_2$O$_3$ supported catalysts. This catalyst also shows higher reduction temperatures and it could affect amount of active sites in catalyst.

CO$_2$ selectivity presents the catalyst activity for water–gas shift reaction and the results clarify that the selectivities are 0.8%, 0.9%, and 0.4% for Co/Al$_2$O$_3$, Co/CNTs, and Co/GNS catalysts. Experimental and theoretical investigations show that the exposed Co edges as the only sites likely to dissociate water [37]. Based on these observations, smaller Co particles provide more active sites for water dissociation instead of water adsorption and lower water–gas shift reaction rate are expected which is in agreement with the presented experimental results for our catalysts.

It is well established that smaller Co particles increase catalyst selectivity toward light products. It can be concluded

that small Co particles are more active in hydrogenation reactions and produce light hydrocarbons [38]. Methane selectivity calculated as 20.9%, 14.4%, and 11.8% for Co/GNS, Co/CNTs, and Co/Al$_2$O$_3$ catalysts, respectively. On the other hand, for these catalysts, C$_5^+$ liquid products calculated as 70.2%, 72.8%, and 79.7%. As the FESEM results show, Co/GNS catalysts have smaller Co particles. The changes of hydrocarbon selectivities are in good agreement with the particle-size trends. Improving the C$_5^+$ selectivity along with CO conversion is one of the most important aims in FTS and for investigated catalysts, and according to the results, CVD acts as a useful method for modifying FTS catalyst activity (Fig. 6).

Anderson–Schultz–Floury (ASF) distribution for FTS products for all catalysts is plotted and presented in Fig. 7. Chain growth probability was determined using C$_3^+$
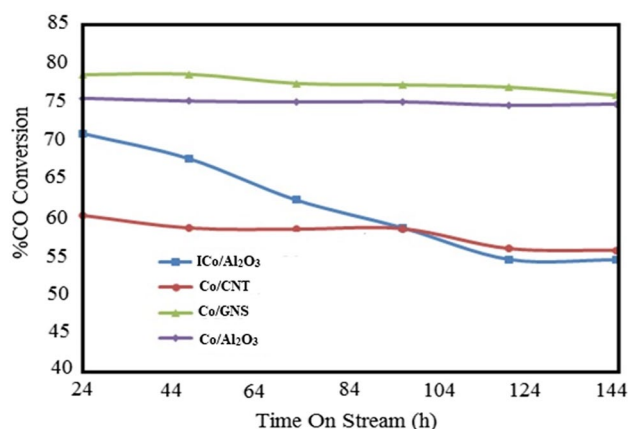
Fig. 8 FTS performance of Co/GNS, Co/CNT, Co/Al$_2$O$_3$, and ICo/Al$_2$O$_3$ catalysts (reaction conditions: 220 °C, 1.8 MPa, H$_2$/CO$=2$, and 0.6 g catalyst)

Fig. 9 Change of selectivity with time-on-stream for Co/GNS, Co/CNT, Co/Al$_2$O$_3$, and ICo/Al$_2$O$_3$ (reaction conditions: 220 °C, 1.8 MPa, H$_2$/CO = 2.0, and 0.6 g catalyst)
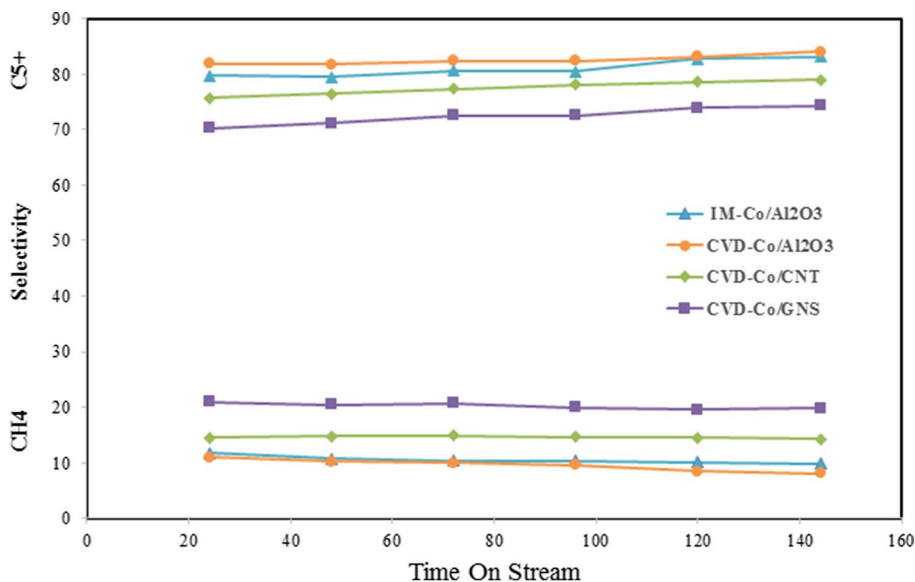
distribution plots and the results are 0.77, 0.79, and 0.83 for Co/GNS, Co/CNTs, and Co/Al$_2$O$_3$ catalysts. These results approve that high-molecular-weight hydrocarbons are produced using Co/Al$_2$O$_3$ catalyst.

Stability of catalysts

Catalyst deactivation is a major challenge in cobalt-based Fischer–Tropsch synthesis. Combined with the relatively high price of cobalt, improved stability of the catalyst will add competitiveness to the technology [39]. The stability of the studied catalysts was studied, and %CO conversion (Fig. 8), methane, and C$_5$$^+$ selectivity (Fig. 7) variations as a function of time-on-stream were measured every 24 h.

As shown in Fig. 8, catalysts prepared by CVD method indicate somehow different deactivation behavior. The activity drops slowly in these catalysts in comparison to the catalyst prepared by impregnation method. In ICo/Al$_2$O$_3$ catalysts, 21.4% decrease in FTS activity was observed during the first 144 h time-on-stream and this amount is reported as 1.3% in Co/Al$_2$O$_3$ catalysts prepared by CVD method. The active metal particle size and their dispersion play a crucial rule in catalyst stability. From this point of view, small and well-dispersed catalysts need longer run time for agglomeration.

The percentage of activity lose is calculated as 6.7% and 3.3% for Co/CNTs and Co/GNS catalysts, respectively. The catalyst metal is more tightly bound to the GNS edge than to the CNTs surface because of the existence of active dangling bonds of edge carbon atoms. Dangling bonds is formed due to the generation of some defects in the initial process for producing carbon-based materials [40, 41]. The number of edge carbon atom in GNS is relatively more than that of CNTs because of the structure. It is established that

the energy barrier of metal atom diffusion is lower on the graphene layer and CNTs sidewall than on the GNS edge. Thus, catalyst metal agglomeration occurs more easily on the CNTs surface, which causes low disparity [4].

The changes in methane and C$_5$$^+$ selectivity are reported in Fig. 9. During 144 h FT synthesis, the C$_5$$^+$ selectivity increased and reached to 74.3%, 79.1%, 84.0%, and 84.0% for Co/GNS, Co/CNTs, and Co/Al$_2$O$_3$ and ICo/Al$_2$O$_3$ catalysts, respectively. These results suggest that the cobalt particles might became slightly larger at longer times on-stream. Also, it is reported that C$_5$$^+$ selectivity can be affected by the amount of water produced at different %CO conversions [42]. Thus, the changes of C$_5$$^+$ selectivity for catalysts also can be affected by the effect of %CO conversion on the hydrocarbon selectivity.

There are several mechanisms for catalyst deactivation. To specify the presence of each mechanism and determine its portion in catalyst deactivation, detailed information is required, and for this stage, we assume that oxidation, sintering of cobalt crystallites, and coke formation are among the most probable causes in the investigated catalysts [43].

Conclusion

Using chemical vapor deposition for preparation of cobalt FTS catalyst increased metal dispersion, decreased metal particle sizes, and improved the percentage reduction of the catalysts. CVD method increased the catalyst activity and shifted the product distribution to lower molecular weight hydrocarbons. Among the catalyst prepared on Al$_2$O$_3$, CNTs, and GNS, cobalt supported on GNS showed the highest %CO conversion. Having higher quantity of cobalt islands with a large ratio of edge and corners to flat

surface provided the desirable active sites for FT reaction over Co/GNS catalyst. Cobalt supported on Al_2O_3 introduced as the most stable catalyst.

References

1. Demirbas A (2007) Progress and recent trends in biofuels. Prog Energy Combust Sci 33(1):1–18
2. Spath PL, Dayton DC (2003) Preliminary screening-technical and economic assessment of synthesis gas to fuels and chemicals with emphasis on the potential for biomass-derived syngas. National Renewable Energy Lab Golden Co, Golden
3. Jahangiri H, Bennett J, Mahjoubi P, Wilson K, Gu S (2014) A review of advanced catalyst development for Fischer–Tropsch synthesis of hydrocarbons from biomass derived syn-gas. Catal Sci Technol 4(8):2210–2229
4. den Breejen JP, Radstake PB, Bezemer GL, Bitter JH, Frøseth V, Holmen A, de Jong KP (2009) On the origin of the cobalt particle size effects in Fischer–Tropsch catalysis. J Am Chem Soc 131:7197–7203. https://doi.org/10.1021/ja901006x
5. Zhang H, Qiu J, Liang C, Li Z, Wang X, Wang Y, Feng Z, Li C (2005) A novel approach to Co/CNTs catalyst via chemical vapor deposition of organometallic compounds. Catal Lett 101:211–214. https://doi.org/10.1007/s10562-005-4893-3
6. Lee D, Jung GS, Lee HC, Lee JS (2006) Methanol synthesis over Pd/SiO_2 with narrow Pd size distribution prepared by using MCM-41 as a support precursor. Catal Today 111(3):373–378
7. Tian Z-Y, Herrenbrück HJ, Mountapmbeme Kouotou P, Vieker H, Beyer A, Gölzhäuser A, Kohse-Höinghaus K (2013) Facile synthesis of catalytically active copper oxide from pulsed-spray evaporation CVD. Surf Coat Technol 230:33–38. https://doi.org/10.1016/j.surfcoat.2013.06.047
8. Serp P, Kalck P, Feurer R (2002) Chemical vapor deposition methods for the controlled preparation of supported catalytic materials. Chem Rev 102(9):3085–3128
9. Dal Santo V, Mondelli C, De Grandi V, Gallo A, Recchia S, Sordelli L, Psaro R (2008) Supported Rh catalysts for methane partial oxidation prepared by OM-CVD of Rh(acac)(CO)₂. Appl Catal A Gen 346:126–133. https://doi.org/10.1016/j.apcata.2008.05.013
10. Cheng K, Ordomsky VV, Virginie M, Legras B, Chernavskii PA, Kazak VO, Cordier C, Paul S, Wang Y, Khodakov AY (2014) Support effects in high temperature Fischer–Tropsch synthesis on iron catalysts. Appl Catal A Gen 488:66–77. https://doi.org/10.1016/j.apcata.2014.09.033
11. Moussa SO, Panchakarla LS, Ho MQ, El-Shall MS (2014) Graphene-supported, iron-based nanoparticles for catalytic production of liquid hydrocarbons from synthesis gas: the role of the graphene support in comparison with carbon nanotubes. ACS Catal 4(2):535–545
12. Karimi S, Tavasoli A, Mortazavi Y, Karimi A (2015) Cobalt supported on graphene—a promising novel Fischer–Tropsch synthesis catalyst. Appl Catal A 499:188–196
13. Tavasoli A, Karimi S, Taghavi S, Zolfaghari Z, Amirfirouzkouhi H (2012) Comparing the deactivation behaviour of Co/CNT and Co/γ-Al_2O_3 nano catalysts in Fischer–Tropsch synthesis.

J Nat Gas Chem 21:605–613. https://doi.org/10.1016/S1003-9953(11)60409-X
14. Tavasoli A, Taghavi S (2014) Enhancement of ruthenium-promoted Co/CNTs nanocatalyst performance using microemulsion technique. Int J Ind Chem. https://doi.org/10.1007/s40090-014-0009-5
15. Parks GA (1965) The isoelectric points of solid oxides, solid hydroxides, and aqueous hydroxo complex systems. Chem Rev 65:177–198. https://doi.org/10.1021/cr60234a002
16. Taghavi S, Asghari A, Tavasoli A (2017) Chemical engineering research and design enhancement of performance and stability of graphene nano sheets supported cobalt catalyst in Fischer–Tropsch synthesis using graphene functionalization. Chem Eng Res Des 119:198–208. https://doi.org/10.1016/j.cherd.2017.01.021
17. Tavasoli A, Sadagiani K, Khorashe F, Seifkordi AA, Rohani AA, Nakhaeipour A (2007) Cobalt supported on carbon nanotubes—a promising novel Fischer–Tropsch synthesis catalyst. Fuel Process Technol. https://doi.org/10.1016/j.fuproc.2007.09.008
18. Khodakov AY, Chu W, Fongarland P (2007) Advances in the development of novel cobalt Fischer–Tropsch catalysts for synthesis of long-chain hydrocarbons and clean fuels. Chem Rev 107:1692–1744
19. Antonio J, Akhavan H, Romero A, Garcia-minguillan AM, Romero R, Giroir-Fendler A, Valverdea JL (2014) Cobalt and iron supported on carbon nano fibers as catalysts for Fischer–Tropsch synthesis. Fuel Process Technol 128:417–424. https://doi.org/10.1016/j.fuproc.2014.08.005
20. Bezemer GL, van Laak A, van Dillen AJ, de Jong KP (2004) Cobalt supported on carbon nanofibers—a promising novel Fischer-Tropsch catalyst. In: Bao X, Xu Y (eds) Natural gas conversion VII. Elsevier, New York, pp 259–264. https://doi.org/10.1016/S0167-2991(04)80061-2
21. Zhong L, Yu F, An Y, Zhao Y, Sun Y, Li Z, Lin T, Lin Y, Qi X, Dai Y, Gu L, Hu J, Jin S, Shen Q, Wang H (2016) Cobalt carbide nanoprisms for direct production of lower olefins from syngas. Nat Publ Gr 538:84–87. https://doi.org/10.1038/nature19786
22. Morales Cano F, Gijzeman OLJ, de Groot FMF, Weckhuysen BM (2004) Manganese promotion in cobalt-based Fischer–Tropsch catalysis. In: Bao X, Xu Y (eds) Natural gas conversion VII. Elsevier, New York, pp 271–276. https://doi.org/10.1016/S0167-2991(04)80063-6
23. Banerjee A, van Bavel AP, Kuipers HP, Saeys M (2017) CO activation on realistic cobalt surfaces: kinetic role of hydrogen. ACS Catal 7(8):5289–5293
24. Tavasoli A, Abbaslou RMM, Trepanier M, Dalai AK (2008) Fischer–Tropsch synthesis over cobalt catalyst supported on carbon nanotubes in a slurry reactor. Appl Catal A 345(2):134–142
25. Hiura H, Miyazaki H, Tsukagoshi K (2010) Determination of the number of graphene layers: discrete distribution of the secondary electron intensity stemming from individual graphene layers. Appl Phys Express 3(9):095101
26. Ferrari AC (2007) Raman spectroscopy of graphene and graphite: disorder, electron–phonon coupling, doping and nonadiabatic effects. Solid State Commun 143(1):47–57
27. Liu J, Ji Q, Imai T, Ariga K, Abe H (2017) Sintering-resistant nanoparticles in wide-mouthed compartments for sustained catalytic performance. Sci Rep 7:41773
28. Jacobs G, Das TK, Zhang Y, Li J, Racoillet G, Davis BH (2002) Fischer–Tropsch synthesis: support, loading, and promoter effects on the reducibility of cobalt catalysts. Appl Catal A 233(1):263–281
29. Varlashkin P (2011) Approaches to quantification of amorphous content in crystalline drug substance by powder X-ray diffraction. Am Pharm Rev 14(1)

30. Saib A, Borgna A, Van de Loosdrecht J, Van Berge P, Geus J, Niemantsverdriet J (2006) Preparation and characterisation of spherical Co/SiO$_2$ model catalysts with well-defined nano-sized cobalt crystallites and a comparison of their stability against oxidation with water. J Catal 239(2):326–339

31. Jacobs G, Ji Y, Davis BH, Cronauer D, Kropf AJ, Marshall CL (2007) Fischer–Tropsch synthesis: temperature programmed EXAFS/XANES investigation of the influence of support type, cobalt loading, and noble metal promoter addition to the reduction behavior of cobalt oxide particles. Appl Catal A 333(2):177–191

32. Poon SW, Wee AT, Tok ES (2012) Anomalous scaling behaviour of cobalt cluster size distributions on graphite, epitaxial graphene and carbon-rich $(6\sqrt{3} \times 6\sqrt{3})$ R30°. Surf Sci 606(21):1586–1593

33. Duffy D, Blackman J (1998) Magnetism of 3d transition-metal adatoms and dimers on graphite. Phys Rev B 58(11):7443

34. Aksoylu AE, Faria JL, Pereira MFR, Figueiredo JL, Serp P, Hierso J-C, Feurer R, Kihn Y, Kalck P (2003) Highly dispersed activated carbon supported platinum catalysts prepared by OMCVD: a comparison with wet impregnated catalysts. Appl Catal A Gen 243:357–365. https://doi.org/10.1016/S0926-860X(02)00556-2

35. Pan X, Fan Z, Chen W, Ding Y, Luo H, Bao X (2007) Enhanced ethanol production inside carbon-nanotube reactors containing catalytic particles. Nat Mater 6(7):507–511

36. Tessonnier J-P, Pesant L, Ehret G, Ledoux MJ, Pham-Huu C (2005) Pd nanoparticles introduced inside multi-walled carbon nanotubes for selective hydrogenation of cinnamaldehyde into hydrocinnamaldehyde. Appl Catal A 288(1):203–210

37. Lu J, Fu B, Kung MC, Xiao G, Elam JW, Kung HH, Stair PC (2012) Coking- and sintering-resistant palladium catalysts achieved through atomic layer deposition. Science (80-) 335:1205–1208. https://doi.org/10.1126/science.1212906

38. Huo C-F, Li Y-W, Wang J, Jiao H (2008) Formation of CH$_x$ species from CO dissociation on double-stepped Co (0001): exploring Fischer–Tropsch mechanism. J Phys Chem C 112(36):14108–14116

39. Fester J et al (2017) Edge reactivity and water-assisted dissociation on cobalt oxide nanoislands. Nature 8:6–13. https://doi.org/10.1038/ncomms14169

40. Seah C-M, Chai S-P, Mohamed AR (2014) Mechanisms of graphene growth by chemical vapour deposition on transition metals. Carbon N Y 70:1–21. https://doi.org/10.1016/j.carbon.2013.12.073

41. Chen X, Zhang L, Chen S (2015) Large area CVD growth of graphene. Synth Met 210:95–108. https://doi.org/10.1016/j.synthmet.2015.07.005

42. Tsakoumis NE, Rønning M, Borg Ø, Rytter E, Holmen A (2010) Deactivation of cobalt based Fischer–Tropsch catalysts: a review. Catal Today 154(3):162–182

43. Kong K-J, Choi Y, Ryu B-H, Lee J-O, Chang H (2006) Investigation of metal/carbon-related materials for fuel cell applications by electronic structure calculations. Mater Sci Eng C 26(5):1207–1210